Controlled Growth of Polyamide Films atop Homogenous and Heterogeneous Hydrogels using Gel-Liquid Interfacial Polymerization

Mengyuan Wang,[1,2] Christopher M. Stafford,[3] Lewis M. Cox,[4] Adrienne K. Blevins,[1,2] Masoud Aghajani,[2] Jason P. Killgore,[5] and Yifu Ding [1,2,]*

M. Wang, A. K. Blevins, M. Aghajani, Prof. Y. Ding
[1] Materials Science and Engineering Program, University of Colorado, Boulder, CO, 80303, USA
[2] Department of Mechanical Engineering, University of Colorado, Boulder, CO, 80309-0427, USA
E-mail: Yifu.Ding@Colorado.Edu

Dr. C. M. Stafford
[3] Materials Science and Engineering Division, National Institute of Standards and Technology (NIST), Gaithersburg, MD, 20899, USA

Prof. L. M. Cox
[4] Mechanical & Industrial Engineering Department, Montana State University, Bozeman, MT,59717-3800, USA

Dr. J. P. Killgore
[5] Applied Chemicals and Materials Division, National Institute of Standards and Technology (NIST), Boulder, CO 80305, USA

Keywords: interfacial polymerization; hydrogel; polyamide barrier layer; thin film composite membranes

Abstract

Controlled growth of crosslinked polyamide (PA) thin films is demonstrated at the interface of a monomer-soaked hydrogel and an organic solution of the complementary monomer. Termed gel-liquid interfacial polymerization (GLIP), the resulting PA films are measured to be chemically and mechanically analogous to the active layer in thin film composite membranes. PA thin films are prepared using the GLIP process on both a morphologically homogeneous hydrogel prepared from poly(2-hydroxyethylmethacrylate) (PHEMA) and a phase-separated, heterogeneous hydrogel prepared from poly(acrylamide) (PAAm). Two monomer systems are examined: trimesoyl chloride (TMC) reacting with m-phenylene diamine (MPD) and TMC reacting with piperazine (PIP). Unlike the self-limiting growth behavior in TFC membrane fabrication, diffusion-limited, continuous growth of the PA films is observed, where both the thickness and roughness of the PA layers increase with reaction time. A key morphological difference is found between the two monomer systems using the GLIP process: TMC/MPD produces a ridge-and-valley surface morphology whereas TMC/PIP produces nodule/granular structures. The GLIP process represents a unique opportunity to not only explore the pore characteristics (size, spacing, and continuity) on the resulting structure and morphology of interfacially polymerized thin films, but also a method to modify the surface of (or encapsulate) hydrogels.

1. Introduction

Interfacial polymerization between a triacid chloride and a diamine is the current state-of-the-art method for producing the selective layer in thin film composite (TFC) membranes.[1-3] Reverse osmosis-based membranes are comprised of a highly crosslinked, fully-aromatic polyamide (PA) that result from the interfacial polymerization of trimesoyl chloride (TMC) and m-phenylene diamine (MPD), whereas nanofiltration-based membranes are comprised of a less crosslinked, semi-aromatic PA that result from the interfacial polymerization of TMC and piperazine (PIP). To create the selective PA layer, an aqueous diamine solution is first absorbed into a porous support, followed by immersion in an organic solution (e.g., hexane) containing a triacid chloride. The polycondensation reaction between the diamine and triacid chloride at or near the oil-water interface produces a highly crosslinked PA layer that can efficiently separate water and ions. The interfacial polymerization process is known to have the following characteristics: it is self-limiting as reactants have to diffuse through a nascent but highly crosslinked PA film, which ultimately leads to ultrathin layers; it occurs just across the oil-water interface within the organic phase due to the slight solubility of the diamine in the organic solvent; and it often produces highly rough surface morphologies that have been associated with increased fouling propensity of these types of membranes.[4-5]

Given the importance of these membranes in addressing the rising challenge of water treatment, numerous efforts have focused on understanding and controlling both the structure and morphology of the PA layers in TFC membranes.[2, 6-9] For example, Karan *et al.* prepared PA nanofilms as thin as 8 nm with reduced surface roughness by limiting the monomer concentrations and extending the reaction times during interfacial polymerization.[6] Tan et al. achieved Turing structures on the PA layers, including both nanoscale spotted and tubed structures, by increasing the viscosity of the aqueous solution and hence slowing down the diffusion of the diamine during the interfacial polymerization.[7] Mariën et al. used an ionic liquid as the organic solvent to reduce the thickness of the interfacial reaction zone, which led

to a relatively smooth PA layer.[10-11] Finally, Ghosh et al. showed that the pore size, degree of hydrophilicity and surface morphology of the porous support had a dramatic impact on the structure and morphology of the interfacially polymerized PA layers.[12]

Recently, we proposed a variant of the interfacial polymerization process, which we termed gel-liquid interfacial polymerization (GLIP), where an organogel consisting of a crosslinked polydimethylsiloxane (PDMS) slab swollen with a solution of TMC in hexane was submerged in an aqueous MPD solution.[13] As in typical interfacial polymerization, the reaction between TMC and MPD occurs just across the interface in the organic phase, which in this case consists of the PDMS organogel. As a result, a homogeneous, hybrid skin layer forms that resembles a semi-interpenetrating PA/PDMS network. The replacement of the organic solution with an organogel allows us to carry out interfacial polymerization on both flat and patterned gel surfaces, as well as tune the hybrid skin layer composition via the GLIP process parameters. The presence of the dense skin layer dramatically improves the gas barrier properties of the PDMS without sacrificing the elasticity and flexibility of the PDMS.

Here, we propose the contrasting geometry using the GLIP process: instead of replacing the organic phase with an organogel, we replace the aqueous phase with a hydrogel. Specifically, both a homogeneous hydrogel and a heterogenous hydrogel are used as supports (and amine reservoir) for the GLIP process. A homogeneous hydrogel does not possess physical pores but rather consists of a swollen polymer network with a mesh size of around a few nanometers, while a heterogeneous gel is comprised of a sponge-like internal microstructure with pore sizes from tens to hundreds of nanometers. This combination allows us to investigate the role of pore size on the interfacial polymerization process, where pore sizes are both above and below the typical range of pore sizes (typically around tens of nanometers) found in traditional supports such as porous polysulfone and polyacrylonitrile.[12]

Unlike the organogel-based GLIP process that forms a semi-interpenetrating hybrid skin layer, the hydrogel-based GLIP process exhibits the formation of a pure PA layer atop the

hydrogel supports. Moreover, unlike interfacial polymerization on porous supports, the PA layers appear to grow continuously with reaction time and thus is not observed to be self-limiting. The characteristics of the PA layer growth are compared with that of both conventional TFC membranes and PA from conventional interfacial polymerization, and differences between homogeneous and heterogenous hydrogels are investigated. This study not only provides additional insights into the growth mechanism that leads to the complex PA layer morphology, but also provides a new and facile method for surface modification of hydrogels.

2. Materials and methods

2.1. Materials

2-Hydroxyethyl methacrylate (HEMA, ophthalmic grade) was purchased from Polysciences Inc (Warrington, PA). All other chemicals and monomers were purchased from Sigma Aldrich, including poly(ethylene glycol) dimethacrylate (PEGDMA, number average molecular mass = 750 g/mol), 2,2-dimethoxy-2-phenylacetophenone (DMPA, 99 %), acrylamide (AAm), N',N'-methylenebisacrylamide (MBAA), ammonium persulfate (APS), N,N,N',N'-tetramethylethylenediamine (TEMED), 1,3-phenylenediamine (MPD), piperazine (PIP, 99.5 %), trimesoyl chloride (TMC, 99 %), triethylamine (TEA, 99.5 %), (+) 10-camphor sulfonic acid (CSA, 99 %), and hexane (anhydrous, 95 %). All chemicals, unless otherwise specified, were used as received. Deionized water was generated from a RiOs-DI water system (MilliporeSigma) with a resistivity of 10 MΩ-cm.

2.2. Hydrogel preparation

Homogeneous hydrogels were formulated based on crosslinked HEMA (PHEMA). A homogeneous liquid mixture of HEMA, PEGDMA (crosslinker, 5 % by mass relative to HEMA), and DMPA (photoinitiator, 1 % by mass relative to HEMA) was achieved after 15 min of sonication. After degassing by sparging with N_2 gas, the mixture was cast into a glass mold with 1 mm thick spacers and irradiated with 365 nm ultraviolet (UV) radiation (20

mW/cm^2) for 15 min using a mercury lamp. The as-cured PHEMA film was then placed into deionized water for 72 h to leach out unreacted species by exchanging water every 12 h. The fully swollen hydrogel sample was cut into 8 mm × 8 mm × 1 mm (W × L × H) pieces and stored in deionized water prior to the GLIP processes. The mechanical properties of the dry PHEMA sample were characterized by Dynamic Mechanical Analysis (DMA, TA Q800), between 20 ^{o}C and 150 ^{o}C at a rate of 2 ^{o}C/min, under a strain amplitude of 0.1 %.

In contrast, a heterogenous hydrogel was prepared based on polymerization/crosslinking of AAm in the presence of water. A homogenous precursor solution containing 20.8 g AAm, 0.015 g MBAA, 0.011 g APS, and 100 g deionized water was prepared and degassed by sparging with N_2 gas for 15 min. Upon the addition of 10 μL TEMED (catalyst for the polymerization process), the precursor solution was poured into a glass mold with 2 mm thick spacers and cured for 30 min under ambient condition. The as-polymerized hydrogel film was immersed in deionized water for 48 h to leach out unreacted species by exchanging the deionized water every 12 h. The PAAm hydrogel sample was then cut into 10 mm × 10 mm × 2 mm (W × L × H) pieces and stored in water prior to the GLIP processes.

2.3. Hydrogel-based GLIP processes

This study used TMC/MPD and TMC/PIP (chemical structures are shown in **Figure 1a**) as model monomer systems for the GLIP process, consistent with the interfacial polymerization process used in TFC membranes.[15] The GLIP processes on both PHEMA and PAAm hydrogel systems are schematically shown in Figure 1b. A PHEMA or PAAm hydrogel sample was swollen in an aqueous solution containing MPD or PIP (2 % by mass), additive CSA (4 % by mass), and catalyst TEA (2 % by mass) for 12 h. The swelling ratio (Q_s) of the hydrogel sample was estimated as,

$$Q_s = (W_s - W_d)/W_d \quad (1)$$

where W_s and W_d are the mass of hydrogel in the swollen and dry states, respectively. Q_s was determined to be 50.1 % for PHEMA hydrogels and 4280 % for PAAm hydrogels after soaking.

Upon removing excess solution from the surface, the monomer-containing hydrogel was quickly immersed in a hexane solution containing TMC (0.2 % by mass) for different amounts of time to form the crosslinked PA layer on the hydrogel surface. The PA/hydrogel sample was then rinsed thoroughly with hexane to remove any unreacted species and dried under ambient conditions for 48 h.

2.4. Characterizations of the polyamide barrier layer

Surface and cross-sectional morphologies of the PA layer formed on the hydrogels were characterized by field-emission scanning electron microscopy (FESEM, JEOL JSM-7401F). The cross-sections were prepared by freeze fracture in liquid nitrogen, and all the samples were coated with a ≈ 5 nm gold layer before SEM measurement.

The thickness of the PA layers formed on PAAm hydrogels was measured by atomic force microscopy (AFM, DI 3100, Bruker) in tapping mode using Si cantilever tips (Veeco, RTESP), after they were separated from the hydrogel surface and transferred onto a silicon wafer. Due to this film transfer method, the bottom surface of the PA film (in contact with the hydrogel) became the top surface on the Si wafer. The thickness of the films was determined by scanning across the edge of the PA layer. Three measurements were carried out for each sample at randomly selected locations, and the average thickness was reported. The PA films formed on PHEMA hydrogel displayed strong adhesion with the PHEMA both in the wet and dry states and thus could not be isolated. Therefore, the thickness of these PA films was estimated from cross-sectional SEM images.

To probe the nanoscale mechanical properties of the PA layer after it was transferred onto a Si wafer, a second AFM (Cypher, Asylum Instruments) was used in fast-force mapping mode. This technique provides rapid force-volume mapping of surfaces, which calculates a spatially-resolved modulus of the sample surface. The probe used for mapping was calibrated by performing a fast-force map on a polystyrene sample with known modulus. A cantilever with a spring constant of 27.8 N/m (PPP-NCLR, Nanosensors) was chosen as it provided sufficient

sensitivity when performing force curves on the sample. An indentation force of 150 nN was chosen for mapping since the resulting indentation depth, 10 nm ± 2 nm, provided sufficient signal for a contact mechanics model to calculate sample modulus. The default Hertz contact mechanics model was used to fit the force curves, using a tip radius of 15 nm, determined from the calibration, as an input into the model. The z-axis in the resulting images represents the surface topography while the color overlay displays modulus.

To probe the effective modulus of the entire PA film, a buckling/wrinkling-based method was employed.[14] In this case, the film needed to be physically transferred to a soft, compliant substrate. This could only be achieved for the PA films formed on PAAm, since the adhesion between the film and the hydrogel was sufficiently low. A PA film formed on PAAm after a reaction time of 15 s was transferred onto a pre-stretched PDMS substrate (10 % tensile strain). The unloading of the pre-strain in the PDMS compressed and wrinkled the stiff PA film. The wrinkle wavelength was determined by AFM and was used to estimate the effective modulus of the PA film.

X-ray photoelectron spectroscopy (XPS) was performed on a Kratos AXIS Ultra DLD spectrometer with a mono-chromated Al Kα source operating at 1486.6 eV and 140 W. The base pressure of the sample analysis chamber was ≈ 2.0×10^{-9} Pa, and spectra were collected from a nominal spot size of 300 μm × 700 μm. Atomic composition was determined from survey scans over a binding energy range of (0 to 1200) eV, pass energy of 160 eV, step size of 0.5 eV, and dwell time of 0.1 s. All XPS data analysis was performed using the CasaXPS software package.

Attenuated total reflection Fourier Transform infrared (ATR-FTIR) spectra were collected on a Thermo Nicolet 6700 with a PIKE VeeMAX II variable angle accessory and a liquid nitrogen-cooled MCT detector. Spectra were collected on a 65° Ge ATR crystal and were averaged over 100 scans. The angle of incidence on the VeeMAX II was set to match the ATR

crystal (65°). A pressure clamp was used to ensure intimate contact between the sample and the crystal.

3. Results and discussion

3.1. Characteristics of the hydrogel reservoirs

It is believed that characteristics of the porous support, typically an ultrafiltration-type membrane, has significant influence over the PA layers formed in TFC membranes.[12] Typically, interfacial polymerization of TMC and MPD results in the so-called ridge-and-valley structures (an example of a commercial membrane is shown in Figure S1a).[15] Li et al. hypothesized that the Marangoni convection of MPD solution from the pores into the TMC solution leads to the formation of the ridge-and-value morphology while simple convection of MPD solution would lead to smooth surface with small nodules.[16] However, it is unclear how pore size of the support affect the formation of the PA layers, particularly when the pore size is out of the typical range used in fabricating commercial TFC membranes. Unlike the porous support, this paper adopts a homogeneous hydrogel and a heterogeneous hydrogel as amine reservoirs for the interfacial polymerization process (Figure 1), which allow us to probe the above question.

PHEMA hydrogels are a typical example of homogenous hydrogel, i.e. no physical pores are present in the swollen state. Instead, homogenous mixing of an aqueous amine solution and PHEMA chains causes a uniform dilation of the PHEMA network, reaching an equilibrium swelling ratio of ≈ 50.1%, estimated using Eq. (1). Accordingly, the average mesh-size of the swollen PHEMA network can be estimated by,[17]

$$\xi = v_{2,s}^{-\frac{1}{3}}\left(\frac{2C_n\bar{M}_c}{M_r}\right)^{1/2} l \qquad (2)$$

where C_n is Flory characteristic ratio (6.9 for PHEMA) and $\upsilon_{2,s}$ is the polymer volume fraction in the swollen hydrogel (calculated to be 0.64 for 5 % mass crosslinker ratio).[18] M_r and $\bar{M}_c$ correspond to the molecular mass of the HEMA repeat unit (M_r = 130 g/mol) and the PHEMA chain between two neighboring crosslinking points, respectively, and l is the length of the carbon-carbon bond in PHEMA backbone (l = 0.154 nm). $\bar{M}_c$ is estimated using the rubber elasticity theory under small deformation,[19]

$$\bar{M}_c = \frac{\rho RT}{G_r} \quad (3)$$

where R is the gas constant, ρ is density of PHEMA (ρ = 1.27 g/cm^3), and G_r is the storage modulus of PHEMA in the rubbery state. Combining Equation (2) and (3) leads to the following expression for the mesh size of the PHEMA hydrogel:

$$\xi = \upsilon_{2,s}^{-\frac{1}{3}}\left(\frac{2C_n\rho RT}{M_r G_r}\right)^{1/2} l \quad (4)$$

From DMA measurements (Figure S2), G_r was determined to be 1.7 MPa ± 0.2 MPa. Accordingly, the mesh size of the swollen PHEMA was estimated using Eqnuation (4) to be 2.5 nm ± 0.1 nm. This value is smaller than the average surface pore size (10 nm to 20 nm) of conventional porous supports used for fabricating TFC membranes. On the other hand, the mesh size is much larger than the molecular size of the MPD and PIP (< 1 nm), which allows them to readily diffuse through the hydrogel and partition into the hexane phase and react with TMC.

In contrast to homogeneous hydrogels, heterogenous hydrogels such as the PAAm hydrogels used here have a sponge-like internal microstructure formed during polymerization/crosslinking in the presence of water. Specifically, the PAAm hydrogels has a Q_s = 4280.0%. The microstructure of PAAm hydrogels have been deduced using methods such as electrophoresis and rheology.[20-21] Those studies concluded that the pore size depends on both the percentage of the polymer in the hydrogel (T%) and percentage of crosslinker in the dry polymer (C%). Stellwagen et al. showed that pore size became independent of C% when

C% was below 2 %.[20] Accordingly, the *T*% and *C*% of the PAAm hydrogel used here are 20 % and 0.07 %, respectively. For *C*% = 0.5 %, the pore size for *T*% =20 % can be estimated using, $370 \times T^{-0.39}$ = 115 nm. Therefore, it can be expected that the PAAm system (*T*% = 20 %, *C%* = 0.07 %) prepared here should have a pore size in the range of 115 nm, which is much larger than the surface pore size on conventional porous supports used for preparing TFC membranes.

3.2. Morphologies and kinetic growth of PA layers through the GLIP process

Figure 2 summarizes the morphologies of the PA layers after GLIP processing on PHEMA hydrogels with varying reaction times, which are clearly distinguished from the smooth and featureless surface of virgin PHEMA (Figure S1b). The feature sizes for all the samples, estimated from the SEM images, are summarized in Table S1. From ATR-FTIR and XPS measurements discussed later, the chemistry of the surface layers is consistent with that of aromatic PA. The formation of PA layers agrees with current understanding that the MPD (PIP)/TMC polymerization zone is just across the interface within the organic phase. In the GLIP process, this means that the reaction is occurring outside the hydrogel, therefore forming the PA layer atop the hydrogel.

The MPD-PA layer formed after 15 s displays a sub-micron crease-like morphology with local nodular structures (Figure 2a). Note that the MPD-PA layer is too thin to be identified in the cross-sectional SEM. The crease structure is caused by the mismatch of shrinkage strain between PHEMA gel and the PA layer upon drying. It has been shown that aromatic PA films derived from MPD/TMC swell marginally in water (e.g. 1.8 % to 11.9 %),[22] which is much lower than the lateral swelling of the PHEMA hydrogels (estimated from 14.1 % to 16.4 %). As reaction time increased, the surface of the MPD-PA layer becomes rougher and the observable features grows larger (over 10 μm after 70 h, Figure S1c), likely masking any surface creases if they are still present. The dominant morphology of both 16-min and 1-h

reaction samples is flat-balloon or ridge-and-valley structures with porous or sponge-like cross-sections (Figure 2b and 2c). Both features are similar to those observed in TFC membranes.[12, 23-25] The MPD-PA/PHEMA interface appears to be free of voids and delamination, which results in strong adhesion that prevents the isolation of the PA layers from the PHEMA in both the wet and dry states. The thickness of the single layer PA, as estimated as half of the edge thickness of the deflated balloons, is ≈ 42 nm for the 16 min-reaction sample, in good agreement with reported value for the commercial reverse osmosis membranes.[12, 24, 26-27]

In contrast to reverse osmosis membranes fabrication by the reaction between TMC and MPD, nanofiltration membranes formed by the reaction between TMC and PIP are much smoother and much thinner.[8, 28-30] These key chemical and morphological differences present an excellent opportunity to study how the GLIP process might be affected by monomer choice (MPD vs PIP). Figure 3d-3f show the morphology of the PIP-PA layers formed on PHEMA. After 15 s reaction, the PIP-PA layer appears very smooth (Figure 2d), showing neither creases nor nodules as observed in MPD-PA layer. The absence of creases indicates that the PIP-PA had a high degree of swelling after the GLIP process, which is consistent with previous studies that have shown PIP-PA layers on commercial nanofiltration membranes could swell by as much as 26.8 %.[22] The high degree of swelling in PIP-PA means that there will be a smaller strain mismatch between the PIP-PA layer and PHEMA substrate upon drying. After 16 min, the PIP-PA layer displays a network-like structure atop a smooth and dense PIP-PA layer (Figure 2e and Figure S1d), which further grows into micron-scale structures after 1 h reaction (Figure 2f). The morphological evolution of the PIP-PA layers on the PHEMA hydrogels is comparable with that on the porous supports.[6, 31]

The results above demonstrate that a homogenous hydrogel with a mesh size of (2 to 3) nm, without physical pores, can effectively serve as a reservoir for a GLIP process that forms PA layers with continued growth in thickness and surface features. **Figure 3** summarizes the

morphologies of both MPD-PA and PIP-PA layers resulted from GLIP process using PAAm hydrogels. The feature sizes estimated from the SEM images are summarized in Table S2. In contrast to the strong adhesion observed for PA/PHEMA systems, the PA layers show very weak adhesion with the PAAm hydrogels due to their high-water content (Q_s = 4280.0%). Such low adhesion allows us to peel off PA layer from PAAm hydrogel, and examine the morphology and properties of both the top surface (in contact with the TMC/hexane solution) and the bottom surface (in contact with the PAAm hydrogel) of the PA layer.

After 15 s reaction, a thin and continuous film of MPD-PA is obtained, with nodule-like structures on both surfaces (Figure 3a). Note that the wrinkles and folds in the SEM image are caused by the film transfer process, which nonetheless indicates that the MPD-PA layer is mechanically robust. After 16 min of reaction (Figure 3b), the top surface is dominated by ridge-and-valley structures, while the bottom surface appears much smoother with randomly distributed open pores. The 1 h sample shows more hierarchical and larger surface features, while the bottom surface is denser with no open pores. Interestingly, such appearance-and-disappearance of open pores on the bottom surface of PA layers was also observed during interfacial polymerization process on porous support.[6, 23, 27] Specifically, the pore-formation on PA layers by GLIP process was only observed at 2 % MPD, but not the lower (0.2 %) and much higher (20 %) MPD concentration.[27] Furthermore, the pores were only observed on the surface of the PA layer that was in direct contact with aqueous phase (comparable to the hydrogels here), regardless of the interfacial polymerization procedure. These pores are believed to correlated with both the internal voids within the PA layer and the rough surface morphology on PA film,[27] as they are the potential entrance for MPD.[32] The morphological evolution of PIP-PA layers formed on PAAm hydrogels (Figure 3d-3f) appears similar to that of MPD system: increase of reaction time leads to rougher films and open pores on the bottom surface only is observed at intermediate reaction time (16 min, Figure 3e). Moreover, the

surface morphology of the PA layers obtained on PAAm is similar to that obtained on PHEMA, but feature size appears smaller. This trend is somewhat consistent with the study showing that much smoother PA films obtained on support-less, liquid-liquid interfacial polymerization.[33]

From cross-sectional SEM images (**Figure 4a** and 4b), the MPD-PA layers are much more porous than both the PIP-PA layers (the 16 min samples are shown in Figure S3) and the MPD-PA layers formed on PHEMA hydrogels (Figure 2c). This comparison is consistent with the observation that PA layers formed on porous supports with larger pores were rougher and more complex.[12] In contrast, PIP-PA layers have a composite type of structure: rough nodules on top of a continuous layer, which was again consistent with the PIP-PA formed on PHEMA hydrogel (Figure 2f).

In comparison, the PA film from support-free interfacial polymerization using similar monomer formulations as this work result in smoother films with very low surface coverage of ridge-and-valley structures.[33] Conversely, Lee et al. observed increased surface roughness as the reaction time increased for interfacial polymerization at the liquid-liquid interface, and the PA exhibited the traditional ridge-and-valley structures.[32] Comparing these findings, it is clear that the formation of ridge-and-valley structures through interfacial polymerization process does not require the pore structures typically seen in porous support used for fabricating TFC membranes. Most significantly, unlike the self-limiting growth of PA layer on porous supports, the GLIP process with both PHEMA and PAAm hydrogels allows continuous growth of the PA layer presumably due to the ample supply of MPD within the hydrogel.

Figure 4c summarizes the thickness of the PA layers as a function of GLIP reaction time. Note that the thickness of the free-standing PA films was determined by AFM scan across the edge of the films after they were transferred onto silicon wafers. Both MPD-PA and PIP-PA films show continuous growth of thickness with increase of reaction time, reaching tens of micrometers after 72 h. At the same reaction time, PIP-PA films appear thicker than the MPD-

PA films. Within the short reaction time (< 60 s), the thickness of the PA films appear comparable with the values obtained from interfacial polymerization process on porous supports with similar monomer concentrations, as included in the Figure 4c.[6] However, PA layers on porous supports normally exhibit self-limiting growth as the data confirmed from using varied concentrations of MPD in a fixed concentration of TMC solution.[34] In another study, the MPD-PA layer formed after 1 min reaction on porous support reached 343 nm ± 82 nm,[27] which was thicker than the MPD-PA layers formed on PAAm hydrogel under identical formulation and reaction time (Figure 4c).

Furthermore, the PA layers formed on PAAm hydrogels appear thicker than those formed on PHEMA hydrogels under identical GLIP conditions. These comparisons suggest that PA layers can grow continuously if monomers are available. The self-limiting growth on porous supports is most likely due to the complete consumption of the monomers. Typically, diffusion-controlled growth mechanism suggests $h\ (t) \sim t^{1/2}$. [4, 35-36] However, the data in Fig. 4c is best fitted with $h\ (t) = A \times t^{b}$, with b = 0.63 (R^2 value of 0.98). The obtained monomer diffusion coefficient for MPD and PIP through corresponding PA layers is $1.0 \times 10^{-12}\ cm^2/s$ and $3.1 \times 10^{-12}\ cm^2/s$, respectively. Koros[37] reported the diffusion coefficient is around 10^{-15} to $10^{-12}\ cm^2/s$ for a molecule with 4-6 carbon to transport through a dense polymer film. The diffusion coefficients obtained here appear to be on the upper bound of the range, which can be attributed to the hiearchical (and porous) structure of the polaymide layers.

3.3. Properties of selected PA layers derived from the GLIP process

In the following section, the chemical properties of the free-standing PA layers were characterized with ATR-FTIR and XPS, while their local and effective mechanical properties were probed with AFM-based measurements and a wrinkling-based method, respectively. Given the large number of samples, measurements were made on samples with 15 s and 16 min reaction times. **Figure 5** shows the IR spectra of the MPD-PA and PIP-PA layers, supported

on PDMS (40:1) substrates, over the range of 1260 cm^{-1} to 1800 cm^{-1} wavenumbers. This spectral range contains characteristic amide vibrational signals, as labelled on the figures. For MPD-PA layers, the spectra display the vibration peaks at 1662 cm^{-1}, 1542 cm^{-1} and 1305 cm^{-1}, mainly associated the Amide I band C=O stretching vibration, Amide II band N-H in-plane bending, and Amide III C-N stretching vibration, correspondingly. The spectra of the two PIP-PA samples display (Figure 5b) Amide I vibration at 1662 cm^{-1}, and in-plane vibration of C-H at 1364 cm^{-1} and 1470 cm^{-1}.[38] Unlike the MPD-PA samples, no vibrational signals for primary and secondary amines are observed for the PIP-PA samples. The assignments of all the peaks for MPD-PA and PIP-PA are listed in Table S3, which are consistent with the vibrational signatures of MPD-PA layers on uncoated reverse osmosis membranes and the PIP-PA layers formed on nanofiltration membranes. [25, 38]

Furthermore, peaks at 1733 cm^{-1} for MPD-PA and 1737 cm^{-1} for PIP-PA are observed and are associated with the C=O stretching in carboxylic acid groups. For both samples, the measurements made with the bottom surface contacting the ATR crystal show stronger signal of carboxyl groups. This is attributed to the fact that hydrolysis of mesoyl chloride groups arising from the PA network is more severe near the hydrogel surface. As a result, higher concentration of carboxyl groups forms near the bottom surface. The sampling depth of the ATR measurements is estimated to be 300 nm at 1600 cm^{-1} wavenumber for PA with a refractive index of 1.5. Therefore, the carboxyl groups appear stronger when the bottom surface of the PA layers is in contact with the ATR crystals. Note that the presence of carboxyl groups in PA layers normally can decrease the salt rejection of the reverse osmosis membranes.[39, 40]

Next, XPS measurements were carried out on selected MPD-PA and PIP-PA films, which were synthesized on PAAm hydrogels. Table 1 summarizes the atomic percentages for C, N and O for the four samples successfully measured. Most importantly, the value of O/N ratio reflects the degree of crosslinking of the PA layers at the surface (sampling depth of XPS is 5

nm to 8 nm): theoretically, the O/N ratio equals 1 for a fully crosslinked PA network and 2 for a linear PA chains of a triacid chloride and a diamine. Sample surfaces originating from nearest the hydrogel surface (bottom) display O/N ratios between 1.2 and 1.4, indicating the bottom surfaces are highly crosslinked with some dangling carboxyl groups, consistent with the ATR-FTIR measurements. For the PIP-PA sample with 15 s reaction time, the O/N ratio of the top surface is 2.2, suggesting that the top surface is less crosslinked and thus contains a higher proportion of linear polyamide oligomers/chains. Such XPS results show that the PA formation reaction is from bottom to top and the longer reaction time leads to a more completely crosslinked PA network. Comparing with O/N ratio of commercial membranes,[25] PA layers formed by the GLIP process require slightly longer reaction times (> 15 s) to have an equivalent O/N ratio, which is one metric of crosslink density in these PA active layers.

Using a wrinkling-based method, the elastic modulus of the free-standing PA layers were measured.[14] A MPD-PA film with 15 s reaction time on a PAAm hydrogel was transferred onto a ^{PDMS} (10:1) surface that was under a 10 % tensile strain. Upon unloading of the PDMS, the MPD-PA film was under a compressive loading and formed periodic wrinkles, which was imaged by AFM (**Figure 6a**). From the wrinkling wavelength, λ, the elastic modulus E_f of the PA film can be estimated using,[14]

$$E_f = 3E_s \frac{(1-\nu_f^2)}{(1-\nu_s^2)} \left(\frac{\lambda}{2\pi h_f}\right)^3 \qquad (7)$$

where E_s is the Young's modulus of the PDMS (1.8 MPa ± 0.2 MPa from DMA measurements), h_f is the thickness of the PA layer, and ν_f and ν_s are the Poisson's ratio of PDMS and MPD-PA, correspondingly. From AFM measurements, λ = 1757 nm ± 48 nm and the MPD-PA layer thickness is 83.6 nm ± 8.7 nm. Assuming ν_f = 0.39, and ν_s = 0.49,[6] E_f of the MPD-PA layer formed after 15 s is estimated to be 0.23 GPa ± 0.27 GPa. This value agrees well with that reported for MPD-PA nanofilms with similar thickness,[6] but is lower than that reported on PA-layers from a composite reverse osmosis membrane (1.4 GPa)[41] and well-known PA from

nylon (≈3 GPa). For thicker PA films (1 μm or above), delamination occurs during the PDMS unloading, and the wrinkling method becomes ineffective.

In addition to the wrinkling method, AFM operated in fast-force mapping mode provides us with a surface modulus map of MPD-PA films. Because the top surface is too rough to perform accurate measurements, only the bottom surface of the MPD-PA with 1 h reaction time was examined. As shown in Figure 6b, the modulus of the MPD-PA appears non-uniform with values ranging around 0.37 GPa, which is close to but noticeably higher than the wrinkling measurements. The discrepancy in the modulus values can be attributed to the fact that wrinkling methods probe the effective modulus of the entire films, while the AFM-based measurements are only sensitive to the effective modulus within the stress field generated by the AFM probe. It is likely that the porosity near the bottom surface as sensed by the AFM measurements is lower than that throughout the entire layer. Nevertheless, the range of modulus values can be rationalized by approximating the porous PA film as an open-pore cellular solid, where the Young's modulus $E^*$is,

$$E^* = E_0 C_1 \left(\frac{\rho^*}{\rho_0}\right)^2 \quad (8)$$

where ρ^* is the effective density of the porous PA, C_1 is a constant ranging from 0.3 to 1, and E_0 and ρ_0 are the Young's modulus and density of the bulk PA, respectively. The effective porosity of the PA film can be calculated as $(1 - \rho^*/\rho_0)$. By using bulk PA Young's modulus from 1.4 GPa to 3 GPa (from aromatic PA on commercial TFC membrane and nylon), the estimated porosity of PA ranges from 24.4 % to 71.7%.

We attempted to measure the permselective properties of the PA layers formed. However, because of the extremely low permeance of the PHEMA hydrogel, no measurable permeate was obtained on the PA/PHEMA hydrogel membranes. On the other hand, free-standing MPD-PA and PIP-PA layers did not have sufficient mechanical strength required for the pressure-driven permeation test. Therefore, dehydration tests were conducted on the PA/PAAm hydrogels after

the GLIP process for 16 min (Figure 6c). The weight ratio was determined by w_t/w_o, where w_t is the weight of PA/PAAM at dehydration state and $w_o$is its original weight. The PAAm hydrogels were uniformly covered with PA. Specifically, for unmodified PAAm hydrogel, the time at which the hydrogel lost 50 % mass ($t_{1/2}$) is ≈ 3.5 h under ambient conditions, while MPD-PA and PIP-PA coated PAAm hydrogels show $t_{1/2}$ = 6.4 h and $t_{1/2}$ = 11.6 h. It is surprising that PIP-PA layers appear to be more effective at reducing the dehydration rate, as PIP-PA normally shows higher permeability than MPD-PA in membrane applications. The observation is nonetheless consistent with the fact that the thickness of PIP-PA-16 min is much larger than that of the MPD-PA-16 min (Figure 4). In addition, it is possible that the porosity of the PIP-PA is lower than that of the MPD-PA. Regardless of the origin, PA layers resulting from the GLIP process can effectively reduce the dehydration rate of the hydrogels, which could be useful for high-temperature application such as the fuel-cell membranes. [42]

4. Conclusion

In this study, we demonstrate controlled growth of PA layers on the surfaces of hydrogels using a gel-liquid interfacial polymerization (GLIP) process. There are similarities between the MPD-based and PIP-based GLIP process: (1) within a few seconds, ultrathin and continuous PA films form atop the hydrogels, consistent with the process of traditional interfacial polymerization of polyamides; (2) diffusion-limited, continuous growth of the PA layers is observed on both a homogenous hydrogel (PHEMA hydrogel with mesh size of ≈2 nm) and a heterogeneous hydrogel (PAAm hydrogel with a mesh size greater than 100 nm); (3) increasing reaction time leads to an increase in both effective thickness and roughness/feature size of the PA layers; (4) formation of open pores on the bottom surface (in contact with hydrogels) occurs only at intermediate reaction time. The main difference between the MPD-based and PIP-based GLIP process is the surface morphology of the PA layers: ridge-and-valley structures for the

MPD-PA layers and nodule/granular structures for the PIP-PA layers. Compared with the homogeneous hydrogels, the heterogeneous hydrogel systems produce thicker and more porous PA layers that can be easily separated from the hydrogels. The study confirms that PA barrier layers can form atop hydrogels without any physical pores as demonstrated in the case of homogeneous gel. The GLIP process, i.e. the use of gels as reaction reservoir, is applicable to other solvent, monomer, or gel systems to form either hybrid skin layers as reported in our earlier study,[13] or form pure polymer layers atop the gels. Such a facile method can be important for applications of gels (homogenous or heterogeneous), elastomers or hydrated polymers where barrier layers are needed, and vacuum-based methods are not applicable.

Acknowledgements MW and YD acknowledge the funding support from the NSF under grant number CBET-126476 and IIP-1432952. MW and MA acknowledge the American Membrane Technology Association (AMTA)/United State Bureau of Reclamation (USBR) fellowships. LC acknowledge the support of the National Research Council (NRC) fellowship at NIST. The authors also gratefully acknowledge the National Science Foundation (NSF) Industry/University Cooperative Research Center for Membrane Science, Engineering and Technology (MAST) at the University of Colorado at Boulder (CU-B) for support of this research via NSF Award IIP 1624602. Publication of NIST, an agency of the US government, not subject to copyright. Certain commercial equipment, instruments, or materials are identified in this paper to specify the experimental procedure adequately. Such identification does not imply recommendation or endorsement by NIST, nor does it imply that the materials or equipment identified are necessarily the best available for the purpose.

Supporting Information

Supporting Information is available from the Wiley Online Library or from the author.

Acknowledgements

MW and YD acknowledge the funding support from the NSF under grant number CBET-126476 and IIP-1432952. MW and MA acknowledge the American Membrane Technology Association (AMTA)/United State Bureau of Reclamation (USBR) fellowships. LC acknowledge the support of the National Research Council (NRC) fellowship at NIST. The authors also gratefully acknowledge the National Science Foundation (NSF) Industry/University Cooperative Research Center for Membrane Science, Engineering and Technology (MAST) at the University of Colorado at Boulder (CU-B) for support of this research via NSF Award IIP 1624602. Publication of NIST, an agency of the US government, not subject to copyright. Certain commercial equipment, instruments, or materials are identified in this paper to specify the experimental procedure adequately. Such identification does not imply recommendation or endorsement by NIST, nor does it imply that the materials or equipment identified are necessarily the best available for the purpose.

Received: ((will be filled in by the editorial staff))
Revised: ((will be filled in by the editorial staff))
Published online: ((will be filled in by the editorial staff))

Reference

[1] G. Y. Chai, W. B. Krantz, *J. Membr. Sci.* **1994,** *93*, 175.

[2] V. Freger, *Langmuir* **2003,** *19*, 4791.

[3] R. J. Petersen, *J. Membr. Sci.* **1993,** *83*, 81.

[4] V. Freger, *Langmuir* **2005,** *21*, 1884.

[5] V. Freger, *J. Appl. Polym. Sci.* **2003,** *88*, 1162.

[6] S. Karan, Z. W. Jiang, A. G. Livingston, *Science* **2015,** *348*, 1347.

[7] Z. Tan, S. F. Chen, C. J. Gao, *Science* **2018,** *360*, 518.

[8] F. A. Pacheco, I. Pinnau, J. O. Leckie, *J. Membr. Sci.* **2010,** *358*, 51.

[9] S. H. Maruf, D. U. Ahn, Y. F. Ding, *J. Membr. Sci.* **2012,** *405*, 167.

[10] H. Marien, I. F. J. Vankelecom, *J. Membr. Sci.* **2018,** *556*, 342.

[11] H. Marien, L. Bellings, I. F. J. Vankelecom, *ChemSusChem* **2016,** *9*, 1101.

[12] A. K. Ghosh, E. M. Hoek, *J. Membr. Sci.* **2009,** *336*, 140.

[13] M. Y. Wang, J. M. Gorham, Y. F. Ding, *ACS Appl. Mater. Interfaces* **2017,** *9*, 28100.

[14] C. M. Stafford, C. Harrison, E. E. Simonyi, *Nature Materials* **2004,** *3*, 545.

[15] A. K. Ghosh, B. H. Jeong, E. M. V. Hoek, *J. Membr. Sci.* **2008,** *311*, 34.

[16] X. Li, K. Y. Wang, T. S. Chung, *Ind. Eng. Chem. Res.* **2012,** *51*, 10039.

[17] N. A. Peppas, J. Z. Hilt, R. Langer, *Adv. Mater.* **2006,** *18*, 1345.

[18] N. A. Peppas, H. J. Moynihan, J. M. Lucht, *J. Biomed. Mater. Res.* **1985,** *19*, 397.

[19] M. Rubinstein, R. H. Colby, *Polymer Physics*. Oxford University Press, New York, **2003**.

[20] N. C. Stellwagen, *Electrophoresis* **1998,** *19*, 1542.

[21] J. Wang, V. M. Ugaz, *Electrophoresis* **2006,** *27*, 3349.

[22] V. Freger, V. *Environ. Sci. Technol.* **2004,** *38*, 3168.

[23] H. Yan, X. Miao, Y. Liu, *J. Membr. Sci.* **2015,** *475*, 504-510.

[24] M. M. Kłosowski, C. M. McGilvery, A. E. Porter, *J. Membr. Sci.* **2016,** *520*, 465.

[25] C. Y. Y. Tang, Y. N. Kwon, J. O. Leckie, *J. Membr. Sci.* **2007,** *287*, 146.

[26] F. Pacheco, R. Sougrat, I. Pinnau, *J. Membr. Sci.* **2016,** *501*, 33.

[27] J. Xu, H. Yan, Y. Q. Liu, *J. Membr. Sci.* **2017,** *541*, 174.

[28] D. Hu, Z. L. Xu, C. Chen, *Desalination* **2012,** *301*, 75.

[29] S. H. Huang, C. J. Hsu, J. Y. Lai, *J. Membr. Sci.* **2008,** *307*, 73.

[30] K. Boussu, J. De Baerdemaeker, B. Van der Bruggen, *ChemPhysChem* **2007,** *8*, 370.

[31] S. H. Maruf, A. R. Greenberg, Y. F. Ding, *J. Membr. Sci.* **2016,** *512*, 50.

[32] J. Lee, A. Hill, S. Kentish, *Sep. Purif. Technol.* **2013,** *104*, 276.

[33] S. J. Park, W. Choi, J. H. Lee, *J. Membr. Sci.* **2017,** *526*, 52.

[34] T. D. Matthews, H. Yan, B. J. Marinas, *J. Membr. Sci.* **2013,** *429*, 71.

[35] J. Ji, J. M. Dickson, B. E. McCarry, *Macrom.* **2000,** *33*, 624.

[36] L. Janssen, K. Tenijenhuis, *J. Membr. Sci.* **1992,** *65*, 59.

[37] W.J. Koros, G.K. Fleming, H.H. Hoehn, Prog. Polym. Sci., **1988,** 13, 339.

[38] C. Y. Y. Tang, Y. N. Kwon, J. O. Leckie, *Desalination* **2009,** *242*, 149.

[39] H. Ozaki, H. F. Li, *Water Res.* **2002,** *36*, 123.

[40] C. Bellona, J. E. Drewes, G. Amy, *Water Res.* **2004,** *38*, 2795.

[41] J. Y. Chung, J. H. Lee, C. M. Stafford, *Nano Letters* **2011,** *11*, 3361.

[42] C. H. Park, S. Y. Lee, Y. M. Lee, *Nature* **2016,** *532*, 480.

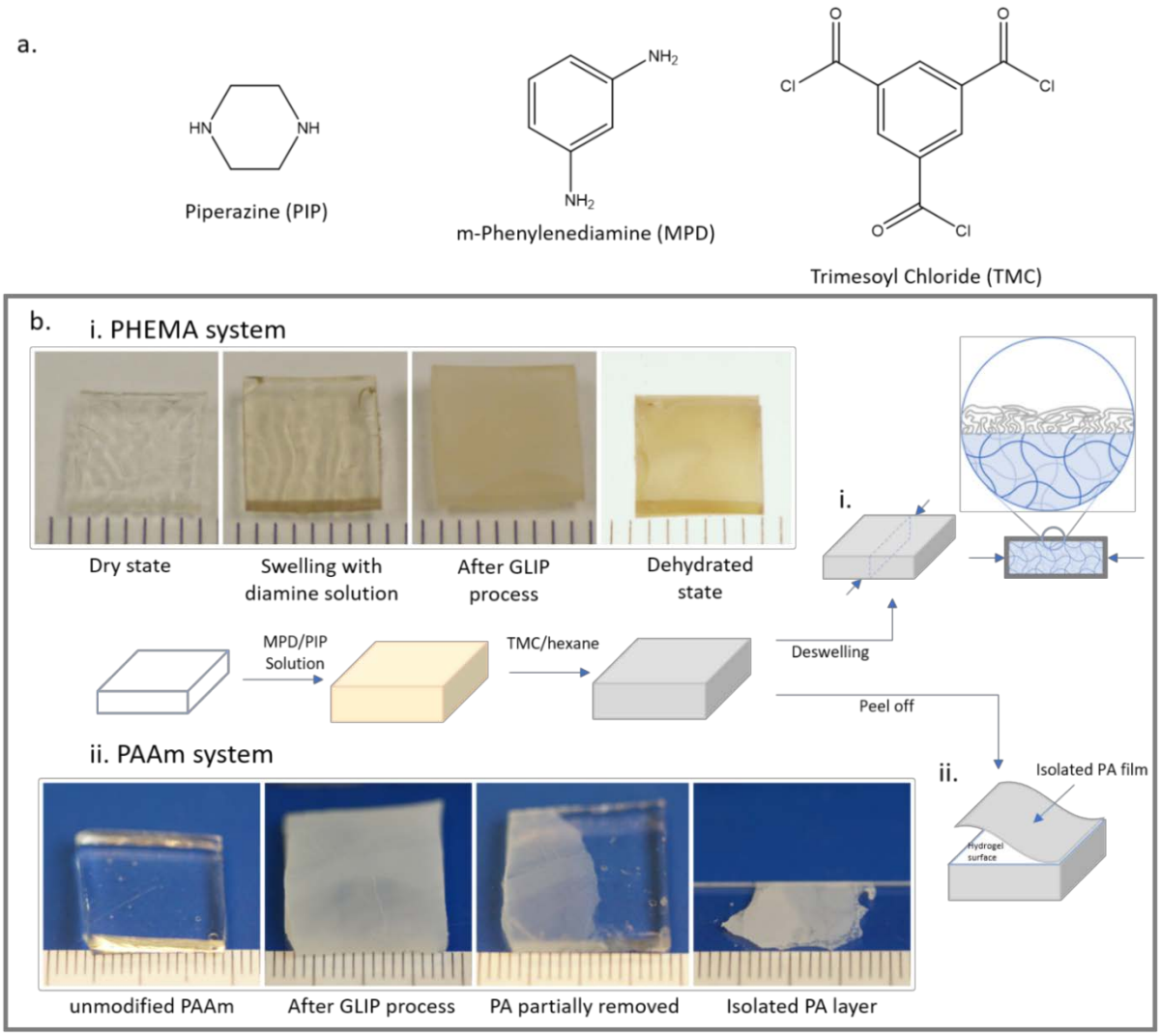

Figure 1. (a) Chemical formulas of monomers used in the GLIP processes. (b) GLIP process on both (i) PHEMA hydrogel and (ii) PAAm hydrogel. Photographs are presented showing the hydrogel samples at different stages of the GLIP process. The tick marks of the ruler in each photo is 1 millimeter.

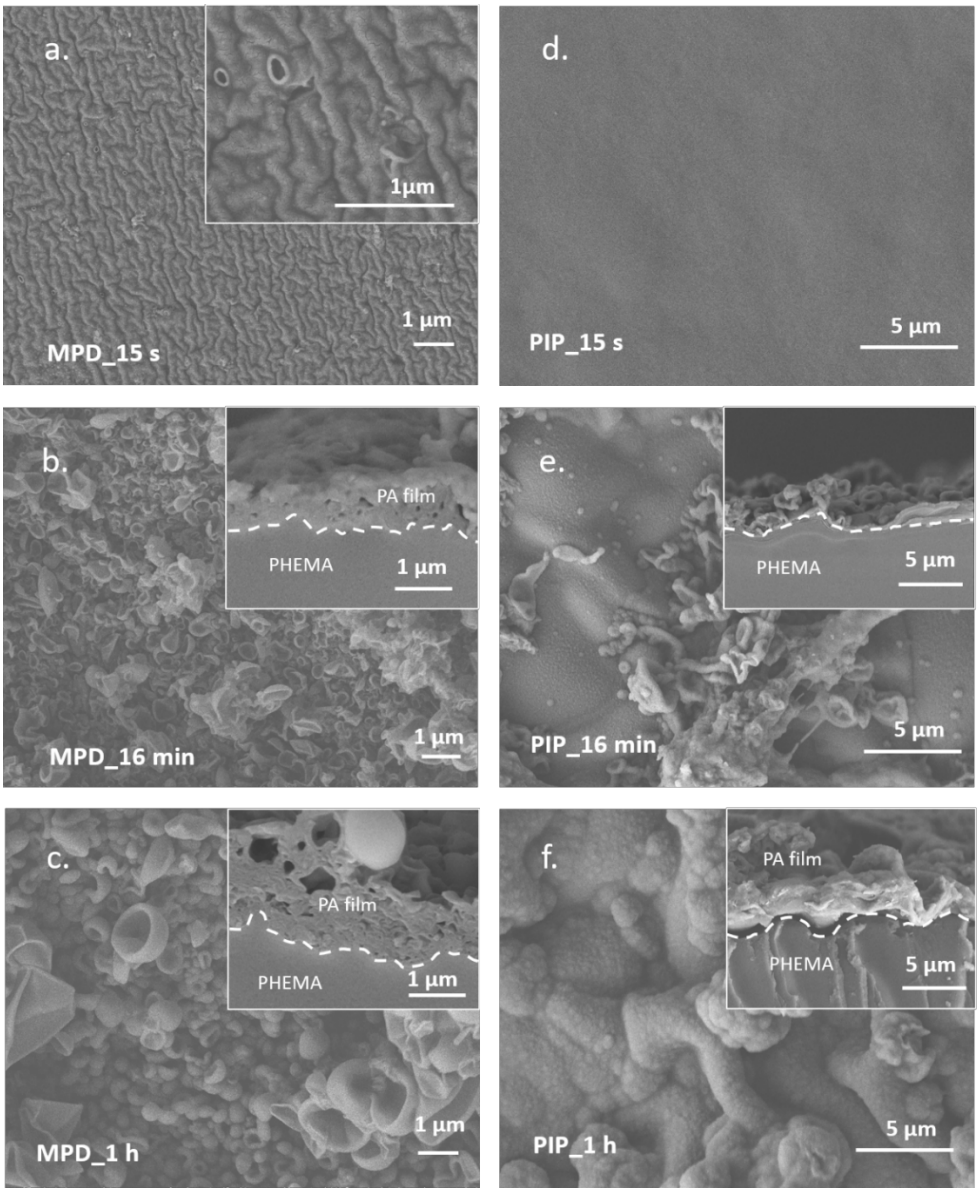

Figure 2. SEM images of the surface of PA layers resulted from the GLIP process on PHEMA hydrogels after different reaction time, using MPD (a-c) and PIP (d-f). Inset of (a) is a higher resolution SEM image, while other insets were cross-sectional SEM images of the corresponding samples.

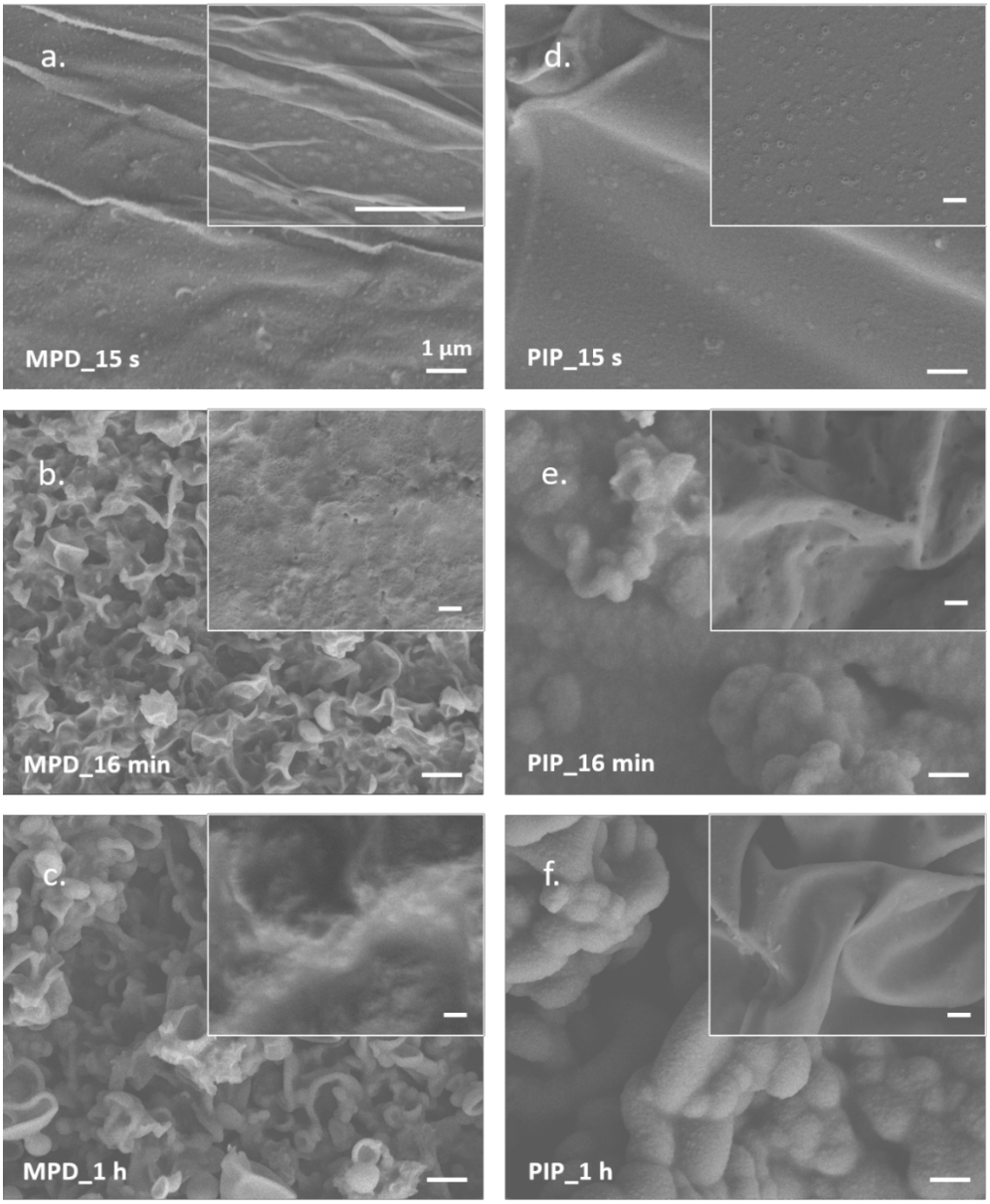

Figure 3. SEM images of the surface of PA layers resulted from the GLIP process on PAAm hydrogels after different reaction time, using MPD (a-c) and PIP (d-f). Insets are SEM images of the bottom surfaces of the PA layers (in contact with the PAAm hydrogel). All scale bars in all images inclding the instes represent a length of 1 µm.

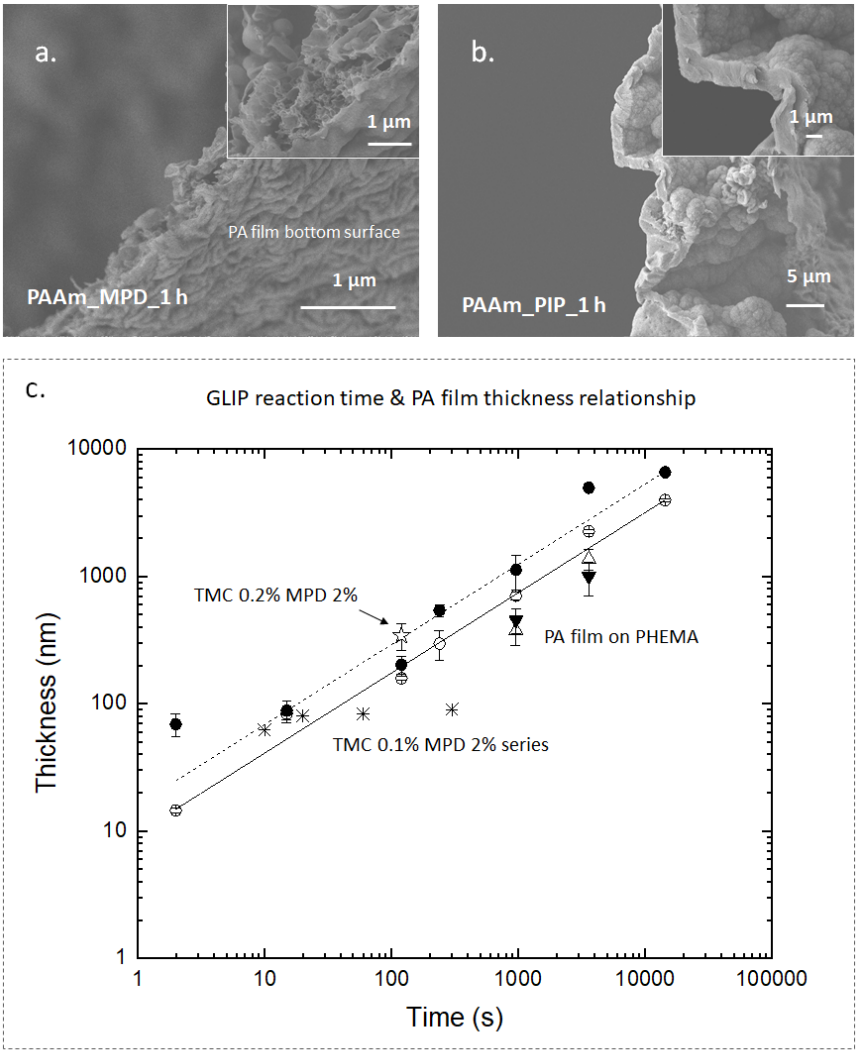

Figure 4. Representative SEM images showing the cross-sections of isolated (a) MPD-PA and (b) PIP-PA layers formed on the PAAm hydrogels after 1 h reaction. (c) Thickness of free-standing MPD-PA (○) and PIP-PA (●) films as function of polymerization time through the GLIP process on PAAm hydrogels. In comparison, thickness for MPD-PA (▼) and PIP-PA (△) formed on PHEMA hydrogels (estimated from cross-sectional SEM images) was included. Also included are thickness of MPD-PA layers formed on porous support using conventional interfacial polymerization process with MPD 2 %/TMC 0.1 % (✳, data from ref. 34) and MPD 2 %/TMC 0.2 % (☆, data from ref. 27). The solid and dash line represent the fitting of MPD- and PIP-based PA film growth with $h_{MPD-PA} = 10.1 \times t^{0.63}$ and $h_{PIP-PA} = 15.1 \times t^{0.63}$ with a $R^2 = 0.98$.

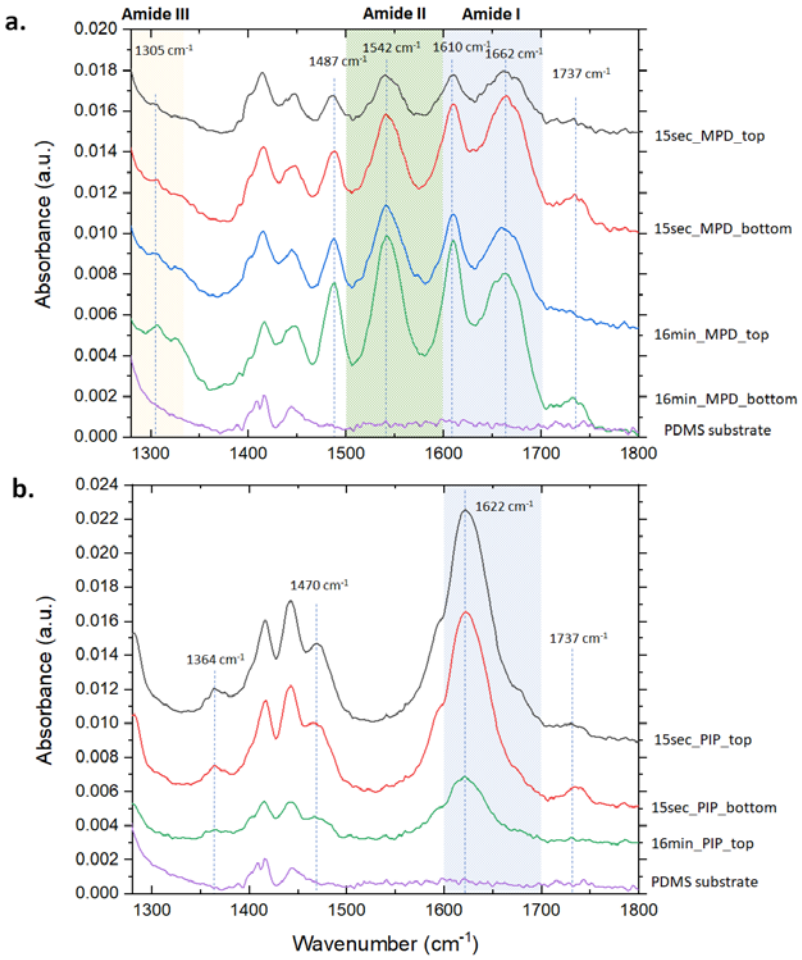

Figure 5. ATR-FTIR spectra of free-standing (a) MPD-PA layers and (b) PIP-PA layers, formed after 15 s and 16 min. Both the bottom and top surfaces were measured. Spectrum of PDMS (40:1) substrate, used to support the PA layers for the measurements, was also included for comparison.

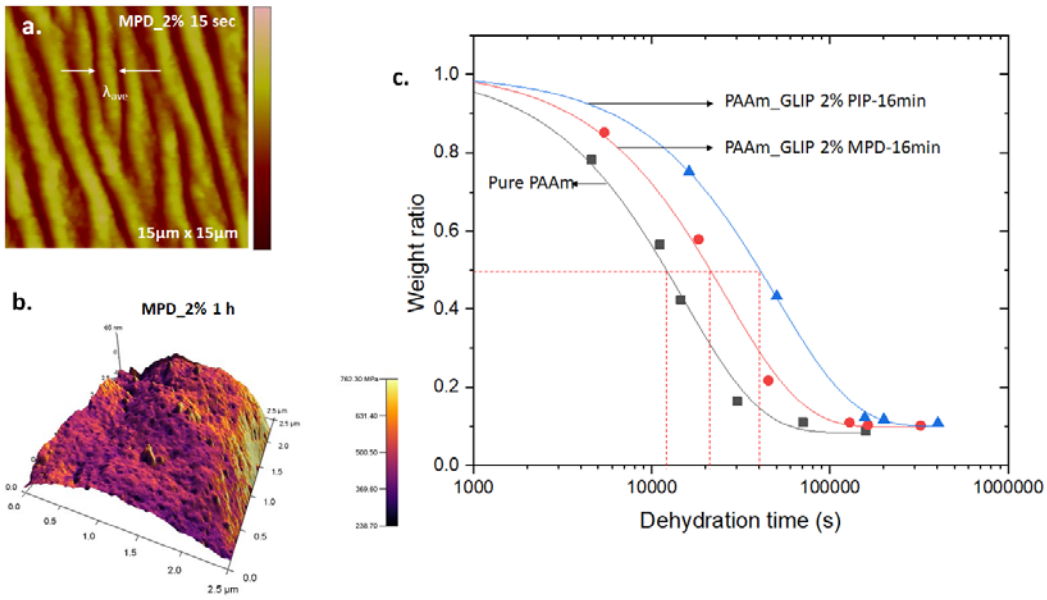

Figure 6. (a) and (b) are mechanical testing of isolated PA layer: (a) nanomechanical measurement by wrinkling phenomenon of MPD_2% 15 sec, and (b) AFM based surface modulus map measurement of MPD_2% 1 h. (c) Dehydration of unmodified PAAm hydrogel and PA-modified PAAm hydrogels.

Table 1. Chemical composition of free-standing PA film top and back side from XPS measurement

Sample	C (%)	N (%)	O (%)	O/N ratio
MPD-16 min-bottom	72.8 ± 1.9	12.5 ± 1.4	14.7 ± 1.1	1.2
PIP-15 s-top	72.0 ± 2.6	11.7 ± 1.2	16.3 ± 1.3	2.2
PIP-15 s-bottom	69.8 ± 1.4	9.8 ± 0.5	20.4 ± 0.6	1.4
PIP-16 min-bottom	72.4 ± 0.8	11.8 ± 0.8	15.9 ± 0.7	1.2

TOC entry

For the first time, controlled growth of polyamide layer is demonstrated using a gel-liquid interfacial polymerization process where hydrogels are used both as a support and a monomer reservoir. On both a homogeneous hydrogel and a heterogeneous hydrogel, the growth kinetics appears to be diffusion limited, in contrast to the self-limiting behaviors commonly observed in interfacial polymerization of polyamide layer for membrane applications.

Keyword Interfacial polymerization of polyamide layer

M. Y. Wang, C. M. Stafford, L. M. Cox, A. K. Blevins, M. Aghajani, J. P. Killgore, Y. F. Ding *

Controlled Growth of Polyamide Films atop Homogenous and Heterogeneous Hydrogels using Gel-Liquid Interfacial Polymerization

ToC figure

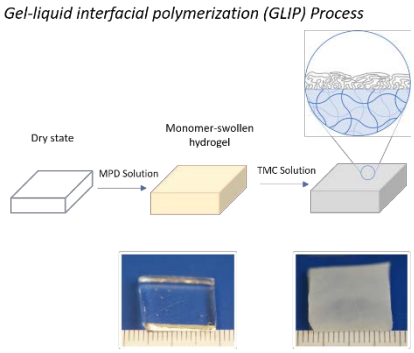

Supporting Information

Controlled Growth of Polyamide Films atop Homogenous and Heterogeneous Hydrogels using Gel-Liquid Interfacial Polymerization

Mengyuan Wang, Christopher M. Stafford, Lewis M. Cox, Adrienne K. Blevins, Masoud Aghajani, Jason P. Killgore, and Yifu Ding *

1. PA film modified poly(HEMA) surface morphology analysis

Table S1. Summary of morphologies of PA film modified poly(HEMA) surface by MPD and PIP

Diamine type	IP reaction time	Surface morphology characteristic	Feature size (nm)
MPD	15 sec	Randomly distributed nodules	Diameter of nodules: 37 ± 14
		Few ridge-and-valley structures	Width of folds: 32 ± 8
		Crease formation on top of bilayer structure	Width of creases: 205 ± 44
	16 min	Flatted balloon structure	Width of folds: 42 ± 11
			Diameter: 283 ± 90
		Large ridge-and-valley structure on top of flatted balloon structure	Size of ridge-and-valley structure: 1843 ± 396
	1 h	Flatted balloon structure	Width of fold: 88 ± 27
			Diameter: 375 ± 62
		Large ridge-and-valley structure on top of flatted balloon structure	Size of ridge-and-valley structure: 1522 ± 354
	2 h	Flatted balloon structure	Width of fold: 136 ± 47
			Diameter: 681 ± 203
		From zoom SEM image, there are nodules on top of ridge-and-valley structure	53 ± 11
	70 h	Flatted balloon structure	Width of fold: 322 ± 68
			Diameter: 11361 ± 4017
	TMV membrane	Ridge-and-valley	Width of fold: 42 ± 6
PIP	15 sec	Smooth surface with no obvious features	
	16 min	Interconnected nodules	Diameter: 1953 ± 461
		Random distributed pores on nodules	Diameter: 162 ± 35
	1 h	Interconnected nodules	Diameter: 1226 ± 223

2. Free-standing PA layer formed on heterogeneous hydrogel

Table S2. Summary of free-standing PA layer morphologies and corresponding feature size.

Diamine type	reaction time	Top surface		Back surface	
		Morphology characteristic	Feature size (nm)	Morphology characteristic	Feature size (nm)
MPD	15 sec	Nodules on smooth film	42 ± 7	Nodules on smooth film	65 ± 9
	16 min	Ridge-and-valley (ridge width)	73 ± 11	Random pores	114 ± 39
		Interconnected leaf-like structure	1029 ± 234		
	1 h	Ridge-and-valley (ridge width)	133 ± 20	Smooth, no pore	--
		Interconnected leaf-like structure	2314 ± 449		
PIP	15 sec	Flat nodules on smooth film	210 ± 74	Random craters inner diameter	87 ± 38
				Random crater ring width	58 ± 23
	16 min	Flat nodules on smooth surface	910 ± 273	Random pores	220 ± 105
		Interconnected nodules	4921 ± 1762		
	1 h	Nodules	1292 ± 291	Smooth, no pore	--

3. ATR-FTIR measurement and composition analysis

Table S3. ATR-FTIR spectra peak assignment of PA film in wavenumber range 1300-1800 cm^{-1}.

sample	FTIR peak wavenumber	Peak assignment
Fully aromatic polyamide	1305 cm^{-1}	Amide III band (C-N stretching vibration only in primary and secondary amide or aromatic amine C-N stretching vibration)
	1487 cm^{-1}	Aromatic in plane ring bend stretching vibration
	1542 cm^{-1}	Amide II band N-H in-plane bending and N-C)
	1610 cm^{-1}	Aromatic amide (N-H deformation vibration or C=C ring stretching vibration)
	1662 cm^{-1}	Amide I band (C=O stretching – dominant contributor, C-N stretching, and C-C-N deformation vibration)
	1733 cm^{-1}	C=O stretching of carboxyl groups
Semi-aromatic polyamide	1364 cm^{-1}	C-H deformation vibration
	1470 cm^{-1}	$-CH_2-CH_2-$ (C-H deformation vibration)
	1622 cm^{-1}	Amide I band (C=O stretching – dominant contributor, C-N stretching, and C-C-N deformation vibration)
	1737 cm^{-1}	C=O stretching of carboxyl groups

4. Surface Roughness as measured by AFM

Table S4. Surface roughness of PA layers as measured by AFM.

Hydrogel type	IP reaction time	RMS roughness (nm)
Homogeneous hydrogel	16 min	361
	1 h	802
	2 h	1152
Heterogeneous hydrogel	16 min	236
	1 h	622

5. Top-down SEM images of virgin hydrogels and PA layers

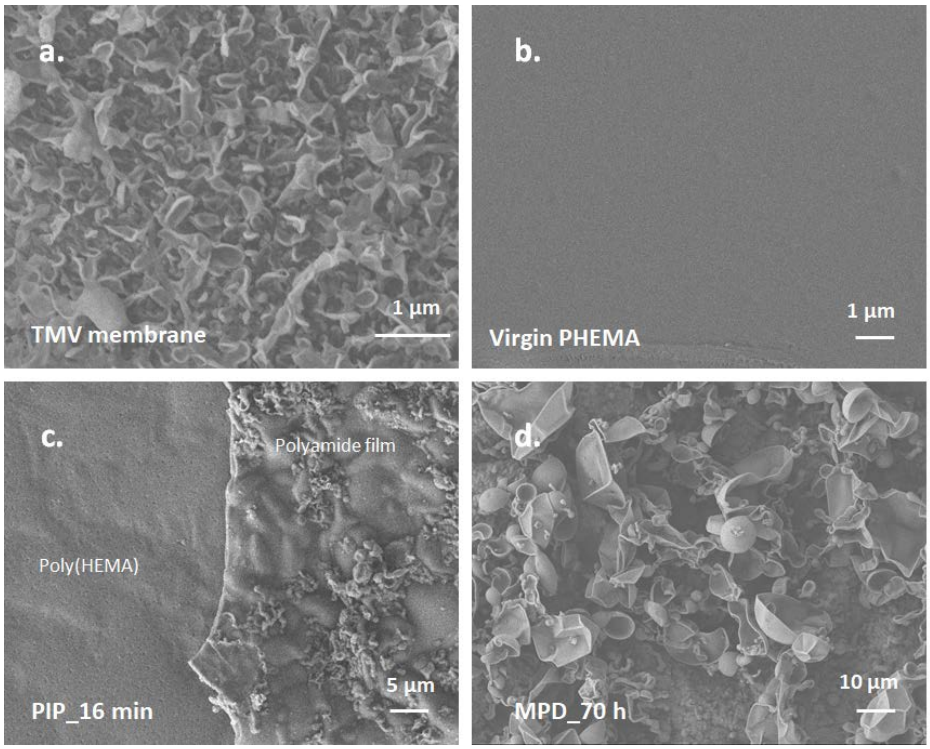

Figure S1. SEM images of the surface of a (a) commercial TFC membrane, (b) virgin PHEMA hydrogel, (c) 16 min PIP-PA on PHEMA hydrogel, where half the layer has been removed, and (d) 70 h MPD-PA on PHEMA hydrogel.

6. 5 % polyHEMA storage modulus in rubbery state by DMA measurement

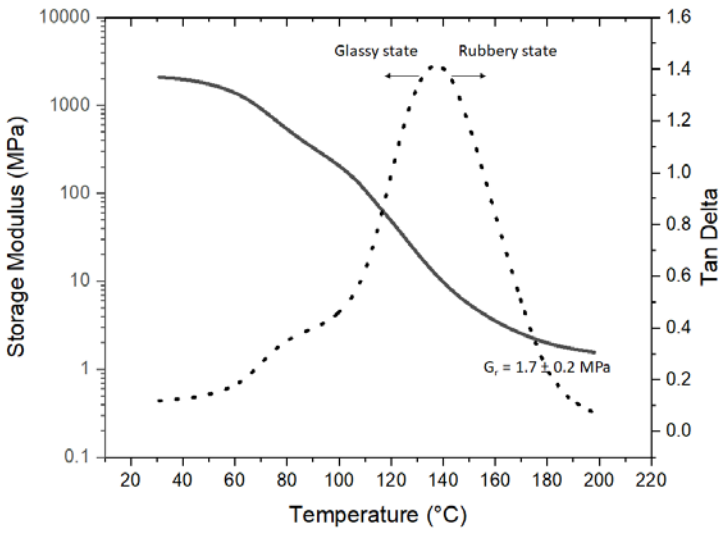

Figure S2. Storage modulus vs. temperature plot of 5 % polyHEMA by DMA measurement.

7. Cross-sectional image of isolated MPD-PA and PIP-PA

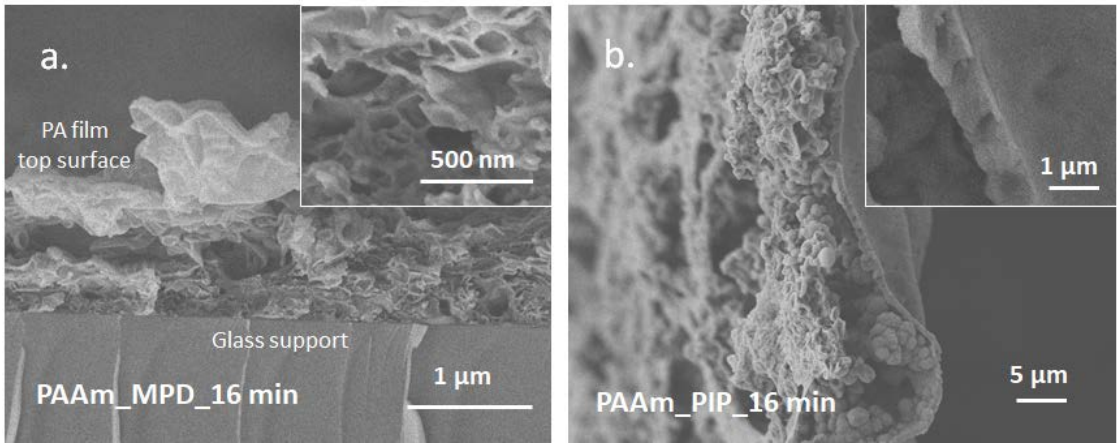

Figure S3. Cross-sectional SEM images of isolated PA layers after 16 min GLIP on a PAAm hydrogel: (a) MPD-PA layer, after transferring to a glass support, and (b) a free-standing PIP-PA layer.